Structure and Stability of the Cu^{II} Complexes with Tandem Repeats of the Chicken Prion

Pawel Stanczak,[‡] Daniela Valensin,[§] Paulina Juszczyk,[||] Zbigniew Grzonka,[||] Caterina Migliorini,[§] Elena Molteni,[§] Gianni Valensin,*[,§] Elena Gaggelli,[§] and Henryk Kozlowski*[,‡]

Faculty of Chemistry, University of Wroclaw, F. Joliot-Curie 14, 50-383 Wroclaw, Poland, Department of Chemistry, University of Siena, via Aldo Moro, 53100 Siena, Italy, and Faculty of Chemistry, University of Gdansk, Gdansk, Poland

Received June 20, 2005; Revised Manuscript Received August 5, 2005

ABSTRACT: Prion protein (PrP) misfolding is one of the pivotal issues in understanding the rudiments of neurodegenerative disorders. The conformational change of mammalian cellular PrP to scrapie PrP is caused by an unknown agent, but there is reasonable evidence supporting the key role of copper ions in this process. The structure of the avian PrP was found to be very similar to the mammalian protein, although there is only 30% homology in the secondary structure. This work shows that copper ions are very effectively bound by hexarepeat fragments of chicken prion protein, although not as effectively as it was found in the case of mammalian protein. By means of potentiometric and spectroscopic techniques (nuclear magnetic resonance, circular dichroism, UV−vis, and electronic paramagnetic resonance), it was shown that Cu^{II} ions coordinate to the chicken PrP hexapeptide domain in physiological pH via imidazole nitrogen donors of His residue(s). The binding pattern changes the structure of peptide involved, indicating a possible impact of Cu^{II} ions in the biology and pathology of nonmammalian PrP, which could be similar to that found for mammalian PrP. The present study shows that, similar to the human prion octapeptide repeats, chicken prion hexapeptide repeats might bind copper ions in two different ways, depending on the number of repeats and metal/ligand molar ratio: (i) an intra-repeat coordination mode in which copper ion is chelated by His imidazole and deprotonated amide nitrogen in monomeric peptide and (ii) an inter-repeat coordination mode in which a polymeric peptide ligand (dimer and trimer) forms polyimidazole complexes that are very stable at physiological pH. Two proline residues inserted into the hexapeptide unit have a critical impact on the metal-binding ability.

Prion proteins (PrPs) have been implicated in diverse human and animal neurodegenerative disorders (*1*). The infectious pathogenesis is usually divided into two phases: (i) the transmission of the PrP pathogenic isoform, its replication with the use of the normal cellular isoform and then propagation of the pathological factor and (ii) the processes connected with various dysfunctions in the infected tissues (*2*). The pathogenic (scrapie) form of the prion protein (PrP^{SC})[1] is formed in a post-translational process, similar to the conformational isoform of the cellular prion (PrP^{C}), the biological function of which is still debated (*3*−*4*). The amino acid sequences of mammalian and avian prion proteins are highly homologous but with a poor identity between glycine- and proline-rich repeat regions. In mammals, the N-terminal domain is very flexible, and it contains characteristic octapeptide repeats (PHGGGWGQ), whereas the similar tandem region in the avian protein contains hexapeptide repeats (PHNPGY) (*5*). The high conservation of these regions across the species ratifies a basic role in the biological function of prions (*6*). The octapeptide repeat fragments can effectively bind Cu^{2+} ions, which seem to play a key role in cell biology, as well as in neurodegeneration (*7*−*9*). Moreover, both full-length chicken and mouse recombinant PrP^{C} retain the same amount of copper and show SOD activity (*10*), abolished by deletion of the tandem repeat region involved in copper binding. These and other findings have been interpreted in terms of PrP^{C} generally acting as a cuproenzyme that plays a direct role in cellular resistance to oxidative stress (*10*).

The binding process of Cu^{II} by the monomeric unit of mammalian octapeptide is well-understood (*8*−*9*, *11*−*14*). The major complex in the physiological pH range is characterized by Cu^{II}, first anchoring at the imidazole nitrogen and then binding two adjacent amide nitrogens of two Gly residues. The Trp side chain is folded back toward Cu^{II} and interacts with a metal-bound water molecule (*11*, *12*). The whole region of octapeptide repeats binds four Cu^{II} ions cooperatively, thus enhancing the ability of PrP^{C} to bind copper (*13*−*15*).

The hexapeptide repeat region of the chicken protein has also been shown to effectively bind Cu^{II}, but a different coordination mode was found compared with the human

* To whom correspondence should be addressed. E-mail: valensin@unisi.it (G.V.); henrykoz@wchuwr.chem.uni.wroc.pl (H.K.).

[‡] University of Wroclaw.

[§] University of Siena.

[||] University of Gdansk.

[1] Abbreviations: NMR, nuclear magnetic resonance; CD, circular dichroism; EPR, electronic paramagnetic resonance; PrP^{C}, cellular prion protein; PrP^{SC}, scrapie prion protein; HPrP, human prion protein; ChPrP, chicken prion protein; DYANA, dynamics algorithm for NMR applications; rmsd, root-mean-square deviation; TOCSY, total correlation spectroscopy; COSY, correlated spectroscopy; ROESY, rotational nuclear Overhauser effect spectroscopy; NOESY, nuclear Overhauser enhancement spectroscopy; HSQC, heteronuclear single-quantum correlation; HMBC, heteronuclear multiple bond correlation.

10.1021/bi051177e CCC: $30.25
Published on Web 09/10/2005

prion octarepeat (*8*, *14*, *16*−*20*). The coordination of the monomeric unit of chicken prion (HNPGYP) is affected by the presence of a Pro residue between Asn and Gly that, of course, impedes deprotonation and binding of two adjacent amide protons. Different Cu^{II}-binding modes in the pH range of 6−8 have been reported: (i) a tetragonal coordination involving two histidine residues and two amide Asn nitrogens in a 1:2 complex resulting into a Cu^{II} coordination comparable to the inter-repeat binding sites of the human peptides (*18*); (ii) an intra-repeat $CuH_{-1}L$ complex, predominant at physiological pH, where copper, first anchored to His imidazole, binds the adjacent Asn amide nitrogen (*17*, *20*). The presence of Pro at position 3 induces binding of phenolate oxygen as a third donor atom (*17*). (iii) Two different intra-repeat $CuH_{-1}L$ complexes depending on the *cis*−*trans* isomerization of the Pro residue in the chain. The most abundant isomer (*trans*-Pro) binds Cu^{II} via the imidazole nitrogen and the deprotonated His amide nitrogen, whereas the Tyr phenolate oxygen adds as a further donor in a minor species (*cis*-Pro) (*19*).

It has recently been reported that the coordination mode of the dimeric Ac-$(PHNPGY)_2$-NH_2 unit toward Cu^{II} consists of two copper ions independently bound to each unit by the imidazolic nitrogen, the deprotonated Asn amide nitrogen, and the Tyr phenolate oxygen (*20*).

The nuclear magnetic resonance (NMR) structure of recombinant chicken prion protein (ChPrP)(23−225) has been solved (*21*), yielding evidence of a C-terminal globular domain and a flexible N-terminal tail of about 100 residues, comprising the hexarepeat region. Therefore, if compared with the human repeat region, the high content of Pro residues in the hexarepeat region does not determine any difference in the secondary structure. However, NMR studies of the N-terminal region of the human prion above pH 6 have revealed a specific structure, made of loops and β-turn-like structures (*22*), which, once compared to the X-ray structure of HGGGW-Cu^{2+} (*11*), was suggested to facilitate binding of copper ions.

In this work, we have used NMR, EPR, CD and UV−vis spectroscopy and potentiometric methods, with the aim of further delineating the structure and stability of Cu^{II} complexes with monomeric, dimeric, and trimeric hexarepeats of chicken prion. Because of the peculiar properties of Pro residues in affecting binding abilities of peptides toward Cu^{II}, the peptides ChPrP(53−58), ChPrP(54−59), ChPrP(54−65), ChPrP(53−70), and ChPrP(54−71) were considered and compared with the aim of ascertaining the eventual impact of the Pro residue at the N terminus on binding features.

MATERIALS AND METHODS

Peptide Synthesis and Purification. All peptides were synthesized according to published methods using standard solid-phase synthesis techniques with a manual methodology (*23*, *24*). Protected amino acids and other chemicals were purchased from Peptide International, Fluka, and Sigma−Aldrich. The resin TentaGel R RAM (Rapp Polymers; capacity of 0.18 mmol/g, 1 g) was treated with piperidine (20%) in dimethylformamide, and all amino acids were linked with the use of DIPCI/HOBt methodology. The coupling reaction time was 1 h. Piperidine (20%) in dimethylformamide was used to remove the Fmoc group at all steps. After deprotection of the last Na-Fmoc group, the peptide resin was washed and treated with *N*-acetylimidazol for 24 h. After the protected peptide resin was washed with methanol, it was dried in vacuo. Then, resin was treated with 10 mL of trifluoroacetic acid/H_2O/phenol/triisopropylsilane (reagent B, 8.8:0.5:0.5:0.2)/1 g of resin at room temperature for 2 h. After filtration of the exhausted resin, the solvent was concentrated in vacuo and the residue was triturated with ether. The crude peptides were purified by reversed-phase high-performance liquid chromatography (RP-HPLC) using a semipreparative Vydac C_{18} column (10 × 250 mm, 5 μm) and a Knauer chromatography system. The aqueous system consisted of 0.1% (v/v) TFA in water solution, while the organic phase was 80% acetonitrile in water, containing 0.08% (v/v) TFA.

The elution was carried out by using a linear gradient from 5 to 50% organic phase in 120 min; the flow rate was adjusted to 15 mL/min; and the separation was monitored by UV absorbency at 223 nm.

In all cases, peptide-containing fractions were analyzed using the analytical Kromasil C_8 column (4.6 × 250 mm, 5 μm) on a Varian Vista 5500 chromatography system using a linear gradient 10−30% organic phase in 20 min. The collected fractions were analyzed using a linear gradient 0−100% organic phase in 60 min (UV detection at 223 nm) and by MALDI−TOF spectroscopy. using a Bruker Biflex III MALDI−TOF mass spectrometer (Bruker Daltonics).

Analytical data were as follows: ChPrP(54−59), Ac-HNPGYP-NH_2, Rt (HPLC) = 15.97 min, M = 724.7 M+ + 1 (MALDI−TOF) = 725.1; ChPrP(53−58), Ac-PHNPGY-NH_2, Rt (HPLC) = 17.30 min, M = 724.7 M+ + 1 (MALDI−TOF) = 725.3; ChPrP(54−65), Ac-HNPGYPHNPGYP-NH_2, Rt (HPLC) = 18.23 min, M = 1390.36, M+ + 1 (MALDI−TOF) = 1391; ChPrP(54−71), Ac-HNPGYPHNPGYPHNPGYP-NH_2, Rt (HPLC) = 18.52 min, M = 2056.04, M+ + 1 (MALDI−TOF) = 2057.8; ChPrP(53−70), Ac-PHNPGYPHNPGYPHNPGY-NH_2, Rt (HPLC) = 20.84 min, M = 2056.04, M+ + 1 (MALDI−TOF) = 2057.5.

Potentiometric Measurements. Stability constants for both proton and Cu^{2+} complexes were calculated from three titrations carried out over the pH range of 3−11 at 298 K using a total volume of 1.5 cm^3. The purities and the exact concentration of the ligand solution were determined by the method of Gran (*25*). NaOH was added from a 0.250 cm^3 micrometer syringe, which was calibrated by both weight titration and the titration of standard materials. The ligand concentration was 1×10^{-3} mol dm^{-3} (for monomers) and 5×10^{-4} mol dm^{-3} (for trimers). The metal/ligand molar ratios were 1:1 for Cu^{2+}−prion monomeric hexarepeats and 1:1, 2:1, and 3:1 for Cu^{2+}−prion trimeric hexarepeats solutions. The pH-metric titrations were performed at 298 K in 0.1 mol dm^{-3} KNO_3 (monomeric forms) and in [30: 70% (v/v) DMSO/water] in 0.1 mol dm^{-3} KNO_3 (trimeric forms) on a MOLSPIN pH-meter system using a normal Russel CMAW 711 semicombined electrode calibrated in proton concentrations using HNO_3 or HNO_3 dissolved in (30: 70%, v/v) DMSO/water, respectively (*26*). The calculated ionic products for water and DMSO/water solutions were 13.770 and 14.501, respectively. The SUPERQUAD and HYPERQUAD 2000 programs were used for the stability constant calculations (*27*, *28*). Standard deviations were

computed by SUPERQUAD and HYPERQUAD 2000 and refer to random errors only. They are, however, good indications of the importance of a particular species in the equilibrium.

Spectroscopic Measurements. Solutions were of similar concentrations to those used in the potentiometric studies, and 30% ethylene glycol was used as a cryoprotectant. Electron paramagnetic resonance (EPR) spectra were recorded on a Bruker ESP 300E spectrometer at X-band frequency (9.3 GHz) in liquid nitrogen. The EPR parameters were calculated for the spectra obtained at the maximum concentration of the particular species for which well-resolved separations were observed. The absorption spectra were recorded on a Beckman DU 650 spectrophotometer. Circular dichroism (CD) spectra were recorded on a Jasco J 715 spectropolarimeter in the 750−240 nm range. The values of $\Delta\epsilon$ (i.e., ϵl−ϵr) and ϵ were calculated at the maximum concentration of the particular species obtained from the potentiometric data. NMR spectra were performed at 14.1 T with a Bruker Avance 600 MHz spectrometer at controlled temperatures (±0.1 K). Solutions were prepared either in water containing 10% deuterium oxide or in 100% deuterium oxide (99.95% from Merck) and were carefully deoxygenated through a freezing/vacuum-pumping/sealing/thawing procedure. The pH was adjusted at desired values with either DCl or NaOD. The desired concentration of copper ions was achieved by using a stock solution of copper nitrate (Sigma Chemical Co.) in deuterium oxide. TSP-d_4, 3-(trimethylsilyl)-[2,2,3,3-d_4] propansulfonate, sodium salt, was used as an internal reference standard. Suppression of a residual water signal was achieved by presaturation or by excitation sculpting, using a selective square pulse on water 2 ms long. A typical NMR spectrum required eight transients acquired with a 9.2 ms 90° pulse, 6600 Hz spectral width, and 2.0 s recycling delay. The assignment was accomplished with total correlation spectroscopy (TOCSY), correlated spectroscopy (COSY), nuclear Overhauser enhancement spectroscopy (NOESY), and rotational nuclear Overhauser effect spectroscopy (ROESY) 2D experiments. TOCSY spectra were recorded with a total spin-locking time of 75 ms using a MLEV-17 mixing sequence. ROESY was performed at a mixing time ranging from 150 to 300 ms, and the radio-frequency strength for the spin-lock field was 1.9 kHz. The spectral width of homonuclear 2D experiments was typically 6000 Hz in both F1 and F2 dimensions. Spin-lattice relaxation rates were measured with inversion recovery pulse sequences. The same sequence was also used to measure the single-selective relaxation rates by means of suitably shaped π pulses instead of the usual nonselective π pulse. All rates were calculated by regression analysis of the initial recovery curves of longitudinal magnetization components, leading to errors not larger than ±3%. While the simple inversion recovery experiment is suitable for the well-isolated peaks, the IR-TOCSY sequence was used to calculate the relaxation rates of the overlapping ^{1}H NMR signal. This was obtained by introducing a ^{1}H 180° pulse followed by a variable delay in front of the TOCSY sequence.

The T_1 values were determined by three-parameter fit of peak intensities to the following equation:

$$I(\tau) = I_0[1 - (1 + B)\exp(-\tau/T_1)]$$

where B is variable parameter that considers nonideal magnetization and which value is smaller than 1. The obtained results were compared with those obtained from a normal IR sequence. The agreement was found in the errors limit of both experiments.

Heteronuclear single-quantum correlation (HSQC) and heteronuclear multiple bond correlation (HMBC) experiments were carried out with standard pulse sequences. Spectral processing was performed on a Silicon Graphics O2 workstation using the XWINNMR 2.5 software.

Molecular Dynamics (MD). All R_1 values, obtained from NMR measurements, were converted into distance constraints (*vide infra*) and used to build a pseudopotential energy for a MD calculation. In this procedure, the potential energy is a function of the difference between the distance constraints provided by the user and corresponding distances found in a given conformer (target function). No other potential energy terms are present except the van der Waals repulsion. At the beginning of the calculation, an arbitrary number of different conformers is generated by randomly varying torsional dihedral angles. Then, the potential energy is minimized by a simulated annealing procedure in the torsion angle space in which the system is brought to a high temperature to allow all possible high-energy starting conformations and subsequently cooled to stabilize it in those potential energy minima that better satisfy the imposed constraints. In particular, we performed the calculation with dynamics algorithm for NMR applications (DYANA) (*29*), using 10 000 steps and 300 random relative starting positions of peptides and Cu^{II}. Because only one molecule can be given as an input in the program, peptides were linked to Cu^{II} through a long chain of linkers without van der Waals radii. These linkers can freely rotate around their bonds and enable us to sample all possible relative positions of the ligand with respect to copper before the minimization step.

The obtained structures were then optimized through an energy minimization followed by a 12 ps restrained MD simulation (2 ps to bring the system from 0 to 298 K, followed by 10 ps at a constant temperature of 298 K), both in a water solvent, using Hyperchem with the MM+ force field. This was done to validate and refine the structure, especially regarding the position of the metal, using a molecular mechanics force field and thus taking into account electrostatic and van der Waals interactions, besides the experimental data. These latter were included by imposing bonds between copper and the atoms involved in its binding and distance restraints for the experimentally obtained copper−proton distances.

RESULTS

The monomeric peptides ChPrP(54−59) and ChPrP-(53−58) were found to behave exactly in the same way either free in solution or upon addition of Cu^{II}. The 600 MHz NMR spectra were performed at pD 7.8, corresponding to the predominance of the single $CuH_{-1}L$ species (*vide infra*). The two Pro residues in the sequence yield four different isomers slowly exchanging between each other; two of them were easily detected and assigned to the *trans*/*trans* (73%) and *trans*/*cis* (27%) isomers [for ChPrP(53−58)] from analysis of ROESY spectra (*19*). Because of the much larger intensity, all NMR results are referred to the main isomer.

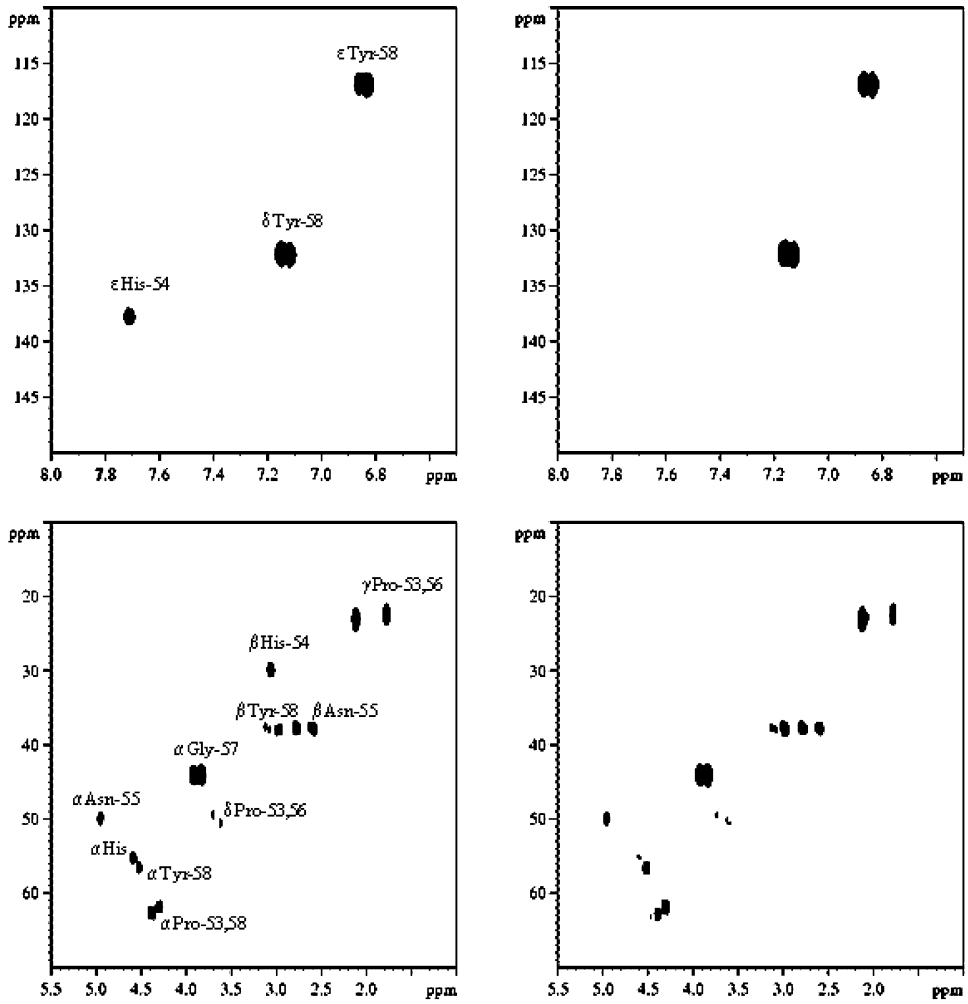

FIGURE 1: ^{1}H-^{13}C HSQC spectra of 4.5 mM ChPrP(53−58) at pD 7.8 and $T = 298$ K before (left) and after (right) the addition of 0.01 equiv of Cu^{II}.

The ^{1}H and ^{13}C assignment is reported in Table 1S in the Supporting Information. The analysis of ROESY spectra showed trivial correlations only, thus excluding the occurrence of any structuring in solution, as usually expected for short peptides.

Addition of the paramagnetic ion caused selective proton and carbon line broadening, which washes out selected connectivities in the ^{1}H-^{13}C HSQC spectra (Figure 1), where ^{1}H-^{13}C correlations related to His-2 diminish in the presence of Cu^{II}: aromatic and β signals completely disappear, while the α cross-peak, although persisting, appears largely reduced in intensity. No effects were observed on Asn-55 α and Tyr-58 aromatic signals. The ^{1}H-^{13}C HMBC spectra (Figure 2) did not show any paramagnetic effects on C_ζ of tyrosine. All of these findings are apparently excluding the involvement of either phenolate or the Asn amide nitrogen in binding Cu^{II}.

The speciation curve based on potentiometric titration for Cu^{II}−ChPrP(53−58) is shown in Figure 3, while protonation and binding constants are summarized in Table 1, together with main spectroscopic features of the various species. Both ChPrP(54−59) and ChPrP(53−58) behave as H_2L acids with protonation sites at the His imidazole nitrogen and the Tyr phenolic oxygen. Four similar Cu^{II} complexes are progressively formed: CuHL, CuL, $CuH_{-1}L$, and $CuH_{-2}L$ (Table 1). The main spectroscopic features of CuHL, appearing at pH ca. 6, are (i) the position of the d−d bands centered at ca. 754 nm, (ii) EPR coupling constants $A_{||} = 138$ or 141 G, and (iii) the EPR g values $g_{||} = 2.349$ or 2.334. The CuHL complex undergoes deprotonation to form the minor CuL species and then the $CuH_{-1}L$ complex dominating in the pH range of 7−9. The d−d bands shift to 650−670 nm, and $A_{||}$ shifts to 176−177 G. In addition, a transition in the 386−415 nm range is detected, although its intensity is relatively small. At pH ≥9.5, the major species becomes $CuH_{-2}L$, with d−d transitions centered at 597 nm and $A_{||} = 197$ G. Two bands that could be assigned to charge-transfer transitions from amide nitrogen and imidazole nitrogen to Cu^{II} ion are situated at 293 and 327 nm, respectively (Table 1) (*30*).

The NMR spectra of the two peptides having respectively two or three HNPGYP repeats did not completely allow us to distinguish among the residues belonging to different units. The proton and carbon chemical shifts were mostly coincident with those of the ChPrP(54−59) peptide and are reported in Table 2S in the Supporting Information. The presence of n Pro residues in the sequence yielded 2^n isomers in slow exchange with each other in the NMR time scale. As in the case of the monomer peptide, the effects of copper were monitored only on the main all-*trans* isomer.

The largest effects induced by copper addition were detected on His residues as shown by the analysis of proton and carbon line broadenings (Figures 4 and 5); in particular,

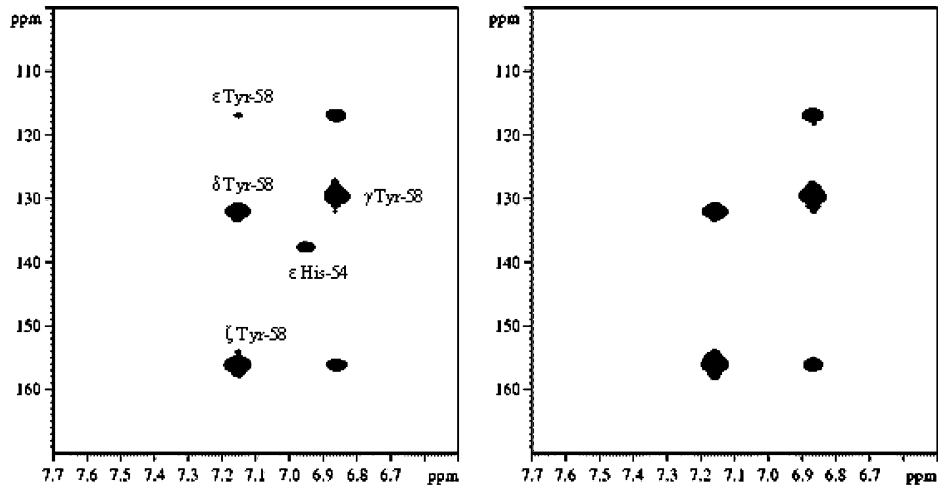

FIGURE 2: ^{1}H-^{13}C HMBC spectra of 4.5 mM ChPrP(53−58) at pD 7.8 and $T = 298$ K before (left) and after (right) the addition of 0.01 equiv of Cu^{II}.

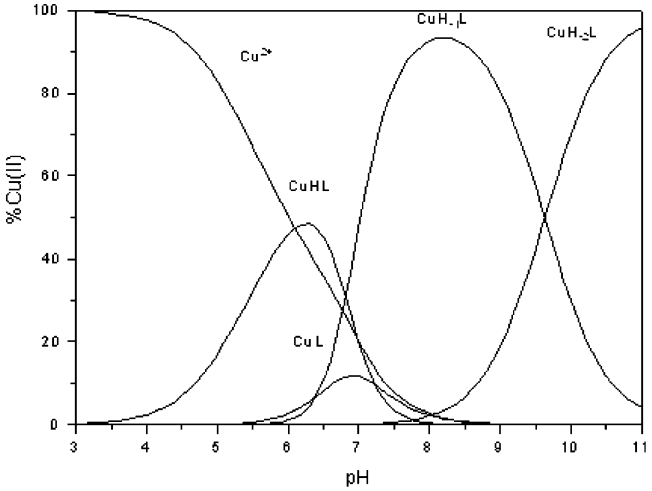

FIGURE 3: Species distribution profile for Cu^{2+} complexes of ChPrP(53−58) at 298 K and $I = 0.1$ M KNO_3. $[Cu^{2+}] = 1 \times 10^{-3}$ M, metal/ligand ratio 1:1.

the intensities of all His resonances, especially those of the aromatic signals, were markedly diminished by the addition of 0.05 equiv of the paramagnetic metal. Unfortunately, the superposition of signals did not allow us to separately calculate the Cu^{II} effects on each His to evaluate their involvement in metal binding. However, the evidence that more copper had to be added to the ChPrP(54−65) and ChPrP(54−71) peptides to obtain the same effects as in aromatic protons of ChPrP(54−59) suggests a slower exchange rate (*31*), a larger metal affinity, and hence, a copper interaction with more than a single unit.

In the case of the dimeric unit, the measurements of R_{1p}, the paramagnetic contribution to the spin-lattice relaxation rate, as defined by eq 1 (Figure 6), showed that His resonances, especially the aromatic ones, were mainly affected by Cu^{II}, whereas almost irrelevant effects were measured for all of the other signals, strongly suggesting the exclusive involvement of His imidazole nitrogens in metal binding.

The obtained R_{1p} values were used to determine the structures of the complexes. It is known that structural delineation of copper complexes with His-containing peptides is only possible provided that the exchange rate from the metal coordination sphere can be evaluated, such that the contribution of T_{1b} to R_{1p} can be extracted (*vide infra*) (*31*). Once the exchange rates were calculated (*vide infra*), all copper−proton distances could be calculated from the R_{1p} values measured in the presence of 0.02 equiv of Cu^{II} (Table 3S in the Supporting Information).

The copper−proton distances were used as the only restraints in molecular modeling of the Cu^{II}−ChPrP(54−65) complex. The simulated annealing protocol was applied to yield a final structure. An energy minimization followed by a MD simulation in the water solvent was performed on this structure to validate and refine it, in particular, concerning the position of the metal, using a molecular mechanics force field, thus taking into account also bond-stretching, angle, and dihedral bending terms and electrostatic and van der Waals interactions, besides some of the NMR-derived distance restraints, which were still included. Figure 7 shows the superimposition of the experimental structure with the energy-minimized one and some snapshots from the MD simulation. The obtained experimental structures (Figure 7A) have a root-mean-square deviation (rmsd) value (taken on the 1−7 residues) of 0.12 ± 0.08 Å for the backbone atoms and 1.46 ± 0.59 Å for the heavy atoms. The proposed structure shows a $2N_{Im}$ donor set.

In the case of the trimeric unit, the R_{1p} values were obtained for His aromatic protons only. The evaluation of the exchange rate (*31*, *vide infra*), however, makes it possible to ascertain which is the imidazole nitrogen ligating the metal ion. In fact, the imidazole H_δ−Cu^{II} distance depends on which nitrogen is bound to the copper(II) ion, such that it can be found at either 0.31 nm (N_ϵ bound) or 0.51 nm (N_δ bound) (*31*). The calculated Cu^{II}−H_δ distance was found in the range of 0.35−0.39 nm (Table 4S in the Supporting Information), which strongly suggests that, among the three His imidazole rings, one binds the paramagnetic ion through N_δ, while the other two bind Cu^{II} through N_ϵ. This still allows three possible binding modes, depending on which of the three histidines in the peptide sequence binds the metal through N_δ.

The models of the three corresponding copper complexes obtained by geometry optimization and a 12 ps MD calculation in water are reported in Figure 8. All energy-minimized final structures were very similar to each other, as suggested by the low rmsd, such that no definite conclusion can be

Table 1

Potentiometric and Spectroscopic Data for Proton and Cu^{2+} Complexes of Ac-HNPGYP-NH_2, 1-Hex
Metal/Ligand Ratio = 1:1; $[Cu^{2+}] = 0.001$ M

			UV−vis		CD		EPR	
species	log β	log K	λ (nm)	ϵ (M^{-1} cm^{-1})	λ (nm)	$\Delta\epsilon$ (M^{-1} cm^{-1})	$A_{\|\|}$ (G)	$g_{\|\|}$
Ac-HNPGYP-NH_2								
HL	9.64 (1)	log $K_{Tyr} = 9.64$						
H_2L	16.02 (1)	log $K_{im} = 6.38$						
CuHL	13.43 (3)		747	20			138	2.349
CuL	6.19 (5)	7.24	minor					
$CuH_{-1}L$	−0.20 (3)	6.39	651	56	705	0.009	177	2.262
					606	0.009		
					386	−0.011		
$CuH_{-2}L$	−9.83 (4)	9.63	597	37	610	0.030	197	2.182
					519	−0.027		
					327	0.041		
					293	−0.274		
					250	1.892		

Potentiometric and Spectroscopic Data for Proton and Cu^{2+} Complexes of Ac-PHNPGY-NH_2, 1-Pex
Metal/Ligand Ratio = 1:1; $[Cu^{2+}] = 0.001$M

			UV−vis		CD		EPR	
species	log β	log K	λ (nm)	ϵ (M^{-1} cm^{-1})	λ (nm)	$\Delta\epsilon$ (M^{-1} cm^{-1})	$A_{\|\|}$ (G)	$g_{\|\|}$
Ac-PHNPGY-NH_2								
HL	9.70 (1)	log $K_{Tyr} = 9.70$						
H_2L	16.01 (1)	log $K_{im} = 6.31$						
CuHL	13.49 (2)		754	20	333	−0.011	141	2.344
					261	0.155		
CuL	6.60 (3)	6.89	minor					
$CuH_{-1}L$	−0.05 (3)	6.65	670	45	690	0.011	176	2.264
					532	0.014		
					415	0.028		
					333	−0.013		
					263	0.487		
$CuH_{-2}L$	−9.59 (2)	9.54	597	37	626	0.080	181	2.254
					536	−0.337		
					463	0.117		
					323	0.088		
					301	0.252		

reached on the His residue that binds Cu^{II} through Nδ.

Potentiometric and speciation curves of the trimeric peptides ChPrP(54−71) and ChPrP(53−70) are shown in Figure 9. Both behave as H_6L acids, and the first dominating copper complex is CuH_3L. The log K values {log K = log β_{CuH3L} − log β_{H3L} = 7.88 [for ChPrP(54−71)] and 7.75 [for ChPrP(53−70)]} are distinctly stronger than those obtained for monomeric hexapeptides and slightly weaker than that of the tetrarepeat (log K = 8.11) (*17*). The d−d transitions are centered at 640−660 nm, and the EPR parameters are $A_{||}$ = 172−178 G and $g_{||}$ = 2.275−2.271 (Table 2). The formation of CuHL, CuL, and $CuH_{-1}L$ complexes results from the successive deprotonations of three Tyr residues. The calculated log K values for the deprotonation reactions: $CuH_2L \rightarrow CuHL \rightarrow CuL \rightarrow CuH_{-1}L$ are 8.76, 9.56, and 10.42 (Table 2). The first value is distinctly lower than those obtained for the metal-free peptide.

At the 2:1 Cu^{II}/peptide ratios, ChPrP(53−70) and ChPrP-(54−71) form eight and nine complexes, respectively (Table 5S in the Supporting Information and Figure 10). ChPrP-(53−70) forms two monomeric species, CuH_4L and CuH_3L, whereas ChPrP(54−71) only forms the CuH_4L species, described above. Both peptides form several complexes with two Cu^{2+} ions bound to one peptide molecule (Table 5S in the Supporting Information and Figure 10). In the pH range of 7−8, the major complex is the Cu_2L species, while at pH >10, the $Cu_2H_{-4}L$ species prevails.

The speciation plots obtained for solutions containing 3:1 Cu^{II}/peptide ratios show some distinct differences between ChPrP(53−70) and ChPrP(54−71) (Figure 11). The position of Pro residues in the peptide sequence is critical for their conformation, and it could be the major reason for the speciation differences.

The competition plot obtained for ChPrP(54−59) and ChPrP(53−58) (Figure 1S in the Supporting Information) indicates that the binding ability of ChPrP(53−58) is slightly larger than that of ChPrP(54−59). Greater differences, however, are easily seen when comparing the binding abilities of ChPrP(54−71) and ChPrP(53−70) in equimolar solutions (Figure 2S in the Supporting Information). At pH <7, the metal-ion-binding abilities are comparable. However, at pH >7, ChPrP(54−71) clearly dominates. The comparison between ChPrP(54−71) and ChPrP(53−70) in coordinating three metal ions shows even larger differences (Figure 3S in the Supporting Information).

DISCUSSION

The addition of paramagnetic Cu^{II} to the solution of either ChPrP(54−59) or ChPrP(53−58) caused similar effects, namely, a selective line broadening in 1D spectra and a selective disappearance of ^1H-^{13}C connectivities in 2D HSQC and HMBC spectra. As largely known, such effects are due to dipolar and scalar coupling of nuclear spins with the Cu^{II} unpaired electron yielding consistent enhancement of lon-

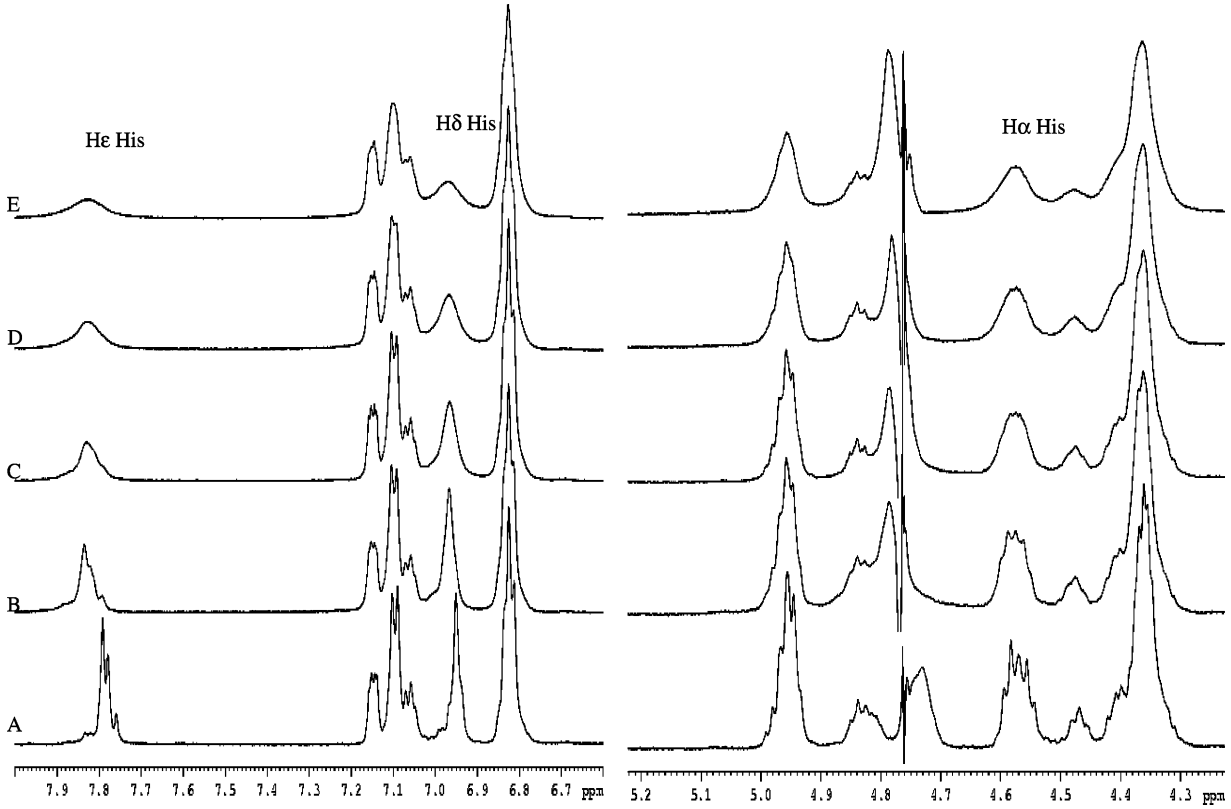

FIGURE 4: ^{1}H 600 MHz spectrum of 6 mM ChPrP(54−71) in D_2O at pD 7.3 and $T = 298$ K: (A) free ligand, (B) after the addition of 0.004 equiv of Cu^{II}, (C) after the addition of 0.01 equiv of Cu^{II}, (D) after the addition of 0.02 equiv of Cu^{II}, and (E) after the addition of 0.05 equiv of Cu^{II}.

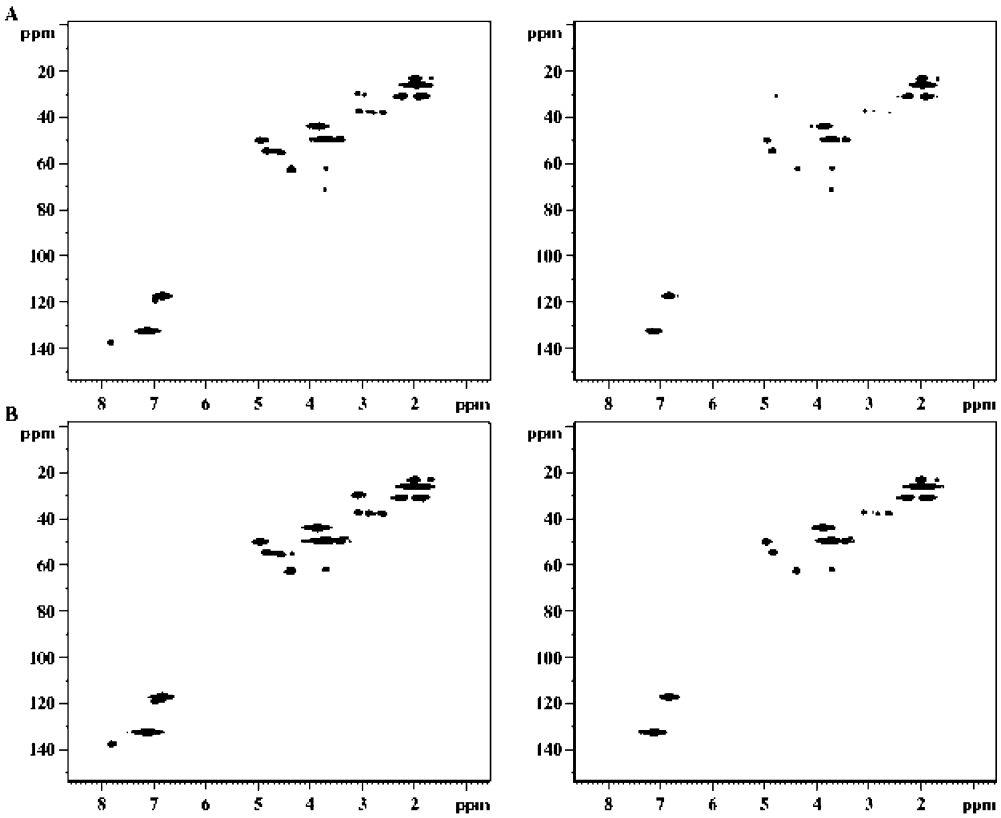

FIGURE 5: ^{1}H-^{13}C HSQC spectra of (A) 6 mM ChPrP(54−65) at pD 7.3 and $T = 298$ K before (left) and after (right) the addition of 0.05 equiv of Cu^{II} and (B) 6 mM ChPrP(54−71) at pD 7.3 and $T = 298$ K before (left) and after (right) the addition of 0.05 equiv of Cu^{II}. The His correlation is shown inside the dashed frames.

gitudinal and transverse relaxation rates of nuclei in the close neighborhood of the paramagnetic ion. In both cases, the paramagnetic effect was mainly limited to all signals belonging to His. In both HSQC and HMBC spectra, the

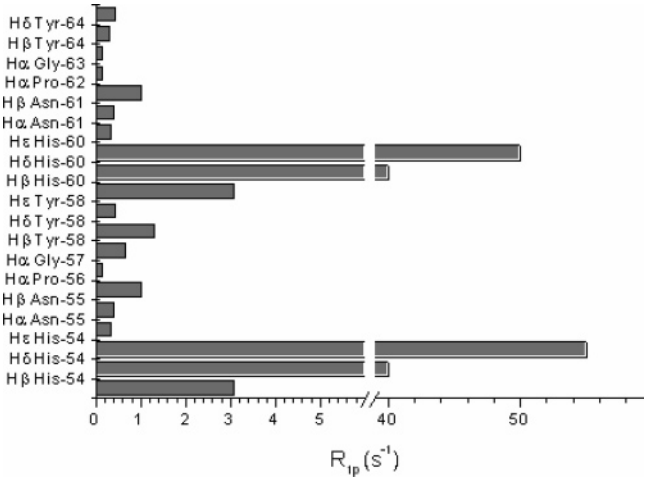

FIGURE 6: Paramagnetic contributions R_{1p} to spin-lattice relaxation rates of selected protons of 2 mM ChPrP(54−65) in H_2O containing 10% D_2O in the presence of 0.02 equiv of Cu^{II} at pH 7.3 and T = 298 K.

correlations related to aromatic and β signals were completely washed out, while the α cross-peak, although persisting, was largely reduced in intensity. The absence of other effects leads to the exclusion of any other residue from participating in metal binding. In particular, (i) the absence of the same effects on Asn α resonances excludes the involvement of this residue in metal coordination, and (ii) the absence of paramagnetic effects on aromatic C_ζ of tyrosine in ^1H-^{13}C HMBC spectra rules the formation of a Cu^{II}−phenolate bond out. This last observation is in apparent contrast with the charge-transfer transition observed in the 386-415 nm range, but it has been recently reported that phenolate binding indeed occurs only in the *trans*−*cis* minor isomer (*19*), consistent with the relatively weak observed intensity of such a transition.

On the basis of all present and previous (*19*) observations, the $CuH_{-1}L$ complex of ChPrP(54−59) and ChPrP(53−58), the major species at physiological pH, is apparently characterized by a coordination mode made of Cu^{II} anchoring first at the imidazole nitrogen and then binding the deprotonated amide group of the same His residue, in contrast with recently reported data (*17*, *18*, *20*) supporting involvement of the Asn amide nitrogen in metal binding, such that the prevalence of intra- over inter-repeat binding can be assessed at least at ≤1:1 Cu^{II}/peptide ratios. The d−d bands at 650−670 nm and the EPR parameters in Table 1 strongly support this $\{N_{im}, N^-\}$ coordination mode (*12*, *17*, *20*, *30*). Lower pH spectroscopic parameters of the CuHL and of the minor CuL species are consistent with Cu^{II} anchored at the imidazole nitrogen only (d−d bands centered around 754 nm) (*12*, *17*, *30*). At pH >9.5, the major $CuH_{-2}L$ species shows parameters typical of three nitrogen donors in the metal coordination sphere; the occurrence of two Pro residues with one preceding His and one following Asn leads us to suppose the additional involvement of Asn in copper binding, probably through its side-chain nitrogen. The d−d transitions centered at 597 nm, $A_{||}$ in the range of 180−200 G, and the lack of the phenolate to Cu^{2+} charge-transfer transition clearly indicate the three nitrogen coordination only (*17*, *30*, *32*). The involvement of the amide and imidazole nitrogen donors is supported by respective charge-transfer transitions at 293 and 327 nm (*vide supra*). The presence of a Pro residue at the N terminus does not affect the coordination mode in the monomeric hexapeptide repeat fragment, and it does not affect the formation of the main $CuH_{-1}L$ complex dominating in the physiological pH range.

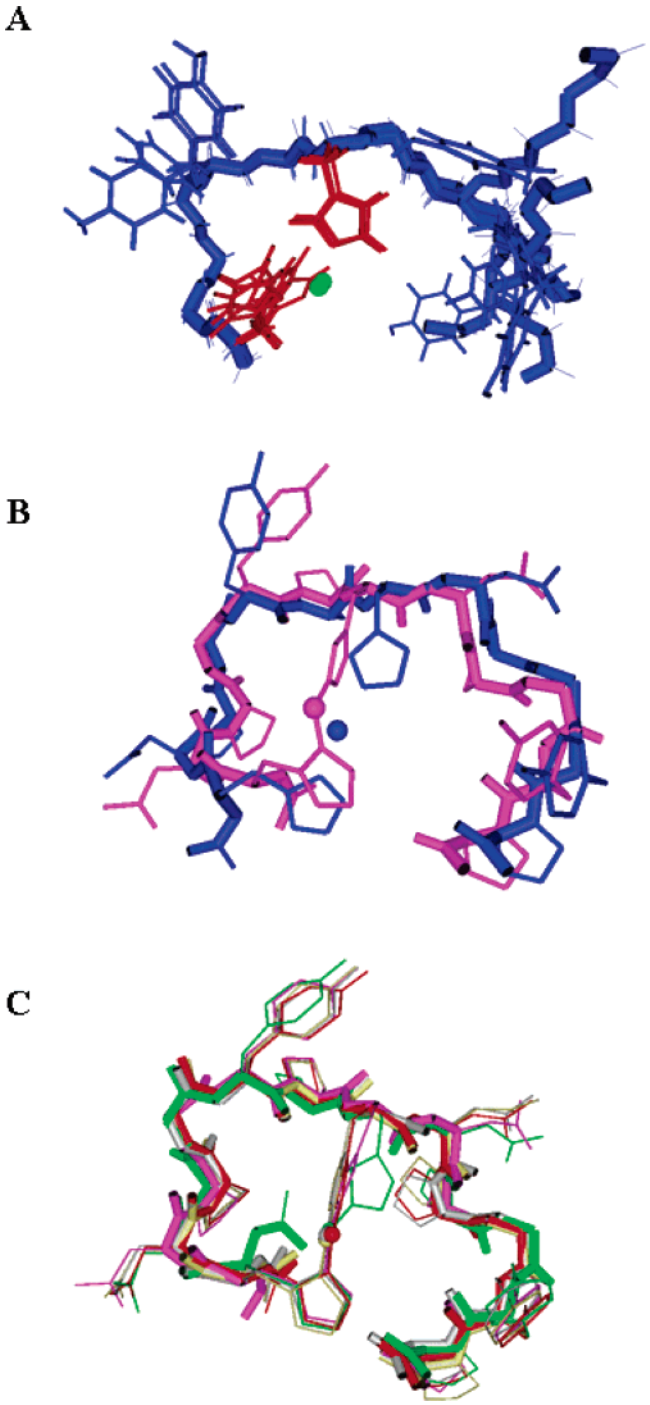

FIGURE 7: (A) Superimposition of the first five structures of the Cu^{II}−ChPrP(54−65) complex obtained from DYANA simulation. (B) Superimposition of Cu^{II}−ChPrP(54−65) structures obtained from experimental data (blue) and from energy minimization (magenta). (C) Superimposition of Cu^{II}−ChPrP(54−65) structures from energy minimization (magenta) and after 12 ps MD calculation (red); the other colored structures represent the snapshots from the MD trajectory. The figure was created with MOLMOL 2K.1.0.

At physiological pH, in both human and chicken repeats, the His imidazole offers a strong anchoring site for copper (*12*, *17*). After the imidazole was anchored, however, copper binding proceeds in a diverse way depending on the analyzed

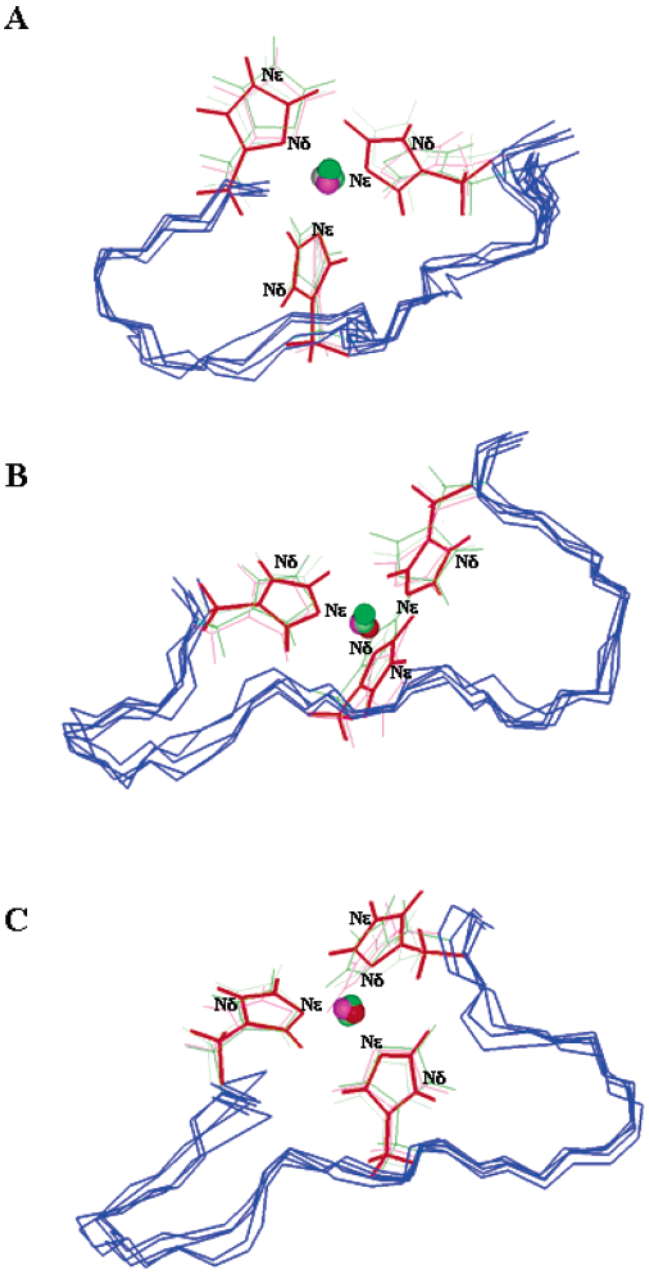

FIGURE 8: Superimposition of Cu^{II}−ChPrP(54−71) structures from energy minimization (magenta) and after 12 ps MD calculation (red); the other colored structures represent the snapshots from the MD trajectory. (A) {N_δ, His-54; N_ϵ, His-60, His-66} Cu^{II} donor set; the rmsd of the structures was 0.71 ± 0.25 Å for backbone atoms and 0.88 ± 0.25 Å for heavy atoms. (B) {N_δ, His-60; N_ϵ, His-54, His-66} Cu^{II} donor set; the rmsd of the structures was 0.72 ± 0.21 Å for backbone atoms and 0.93 ± 0.25 Å for heavy atoms. (C) {N_δ, His-66; N_ϵ, His-54, His-60} Cu^{II} donor set; the rmsd of the structures was 0.75 ± 0.23 Å for backbone atoms and 0.89 ± 0.25 Å for heavy atoms. The figure was created with MOLMOL 2K.1.0.

chicken or human prion repeats because of the presence of a further Pro residue in the chicken repeat. In fact, the Pro residues constitute a "break point" in the peptide sequence that drastically changes copper complexation (*33*−*35*). In the case of human prion octarepeat, where a proline precedes the His residue, the usual simple stepwise coordination of consecutive amide nitrogens is no longer possible and Cu^{II} binding involves the deprotonated amide nitrogens of the following Gly residues (*8*−*9*, *11*−*14*). Such a coordination mode is rather unusual; as for the planar complex, the formation of a less favorable seven-membered {N_{Im}, N^-} chelate ring is necessary.

In the case of the chicken repeat, PHNPGY, two Pro residues are present: one preceding the His residue as in the human repeat and the other in the fourth position in place of the second Gly of the human octarepeat. As a consequence, after anchoring at imidazole, coordination of two amide nitrogens belonging to the residues following His is no longer possible, and this is ratified by the observed binding mode of the chicken repeat involving only one amide nitrogen. Because of the larger stability offered by six- over seven-membered chelate rings, coordination of His rather than Asn amide nitrogen might be expected, and it is indeed supported by all of the data reported here.

As stated elsewhere (*31*, *36*, *37*), additional information on Cu^{II} complexes can be gained by measuring the exchange rate, k_{off}, of the His-containing peptide from the metal coordination sphere. Such a value is in fact easily determined by the proton paramagnetic relaxation enhancement (R_{1p}) of His H_ϵ, because the H_ϵ−Cu^{II} distance is fixed at 0.31 nm, independently of N_δ or N_ϵ bound to the metal.

In fact, the value of R_{1p} is given by the following equation (*38*):

$$R_{1p} = R_{1obs} - p_f R_{1f} = \frac{1}{T_{1obs}} - p_f \frac{1}{T_{1f}} = \frac{p_b}{T_{1b} + k_{off}^{-1}} \quad (1)$$

where k_{off} is the kinetic rate constant for exchange from the metal coordination sphere, p_f and p_b are the fraction of free and bound peptide, R_{1obs} and R_{1f} are the spin−lattice relaxation rates measured, respectively, after the addition of copper and in the metal-free solution, and T_{1b} is the longitudinal relaxation time of ligand nuclei in the metal coordination sphere, given by the Solomon equation (*39*).

The values obtained for ChPrP(54−59) and ChPrP(53−58) measured at pD 7.8 (k_{off} = 5.00 ± 0.70 ms^{-1} in both cases) are faster than that found for the human prion octapeptide PHGGGWG (*31*), suggesting either a different kinetics, a weaker affinity for copper, or both; this is in agreement with the different copper coordination mode observed for the two peptides.

For the CuH_3L complexes of the peptides containing two and three repeats, the evaluation of the exchange rates at different metal ratios (Table 3) shows that increasing the repeat number determines a decrease in k_{off}, strongly supporting the involvement of two and three His imidazole rings in coordination of ChPrP(54−65) and ChPrP(54−71), respectively.

Such behavior is ratified by all other potentiometric and spectroscopic investigations. In particular, a comparison of the log *K* values obtained for the trimer and monomer repeats indicates that ChPrP(54−71) and ChPrP(53−70) have a stronger copper affinity than ChPrP(54−59) and ChPrP(53−58). The values of the stability constants obtained for the complexes with imidazole coordination only clearly indicate the multi-imidazole binding pattern (see also ref *17*). The log *K** value for the metal ion binding to one imidazole in CuHL [L = ChPrP(54−59) or ChPrP(53−58)] species is 3.79, while that for one copper ion with three imidazoles in the CuH_3L [ChPrP(54−71)] complex is 7.48−7.75. The very high increase of the metal-ion-binding ability must then derive from the multi-imidazole coordination.

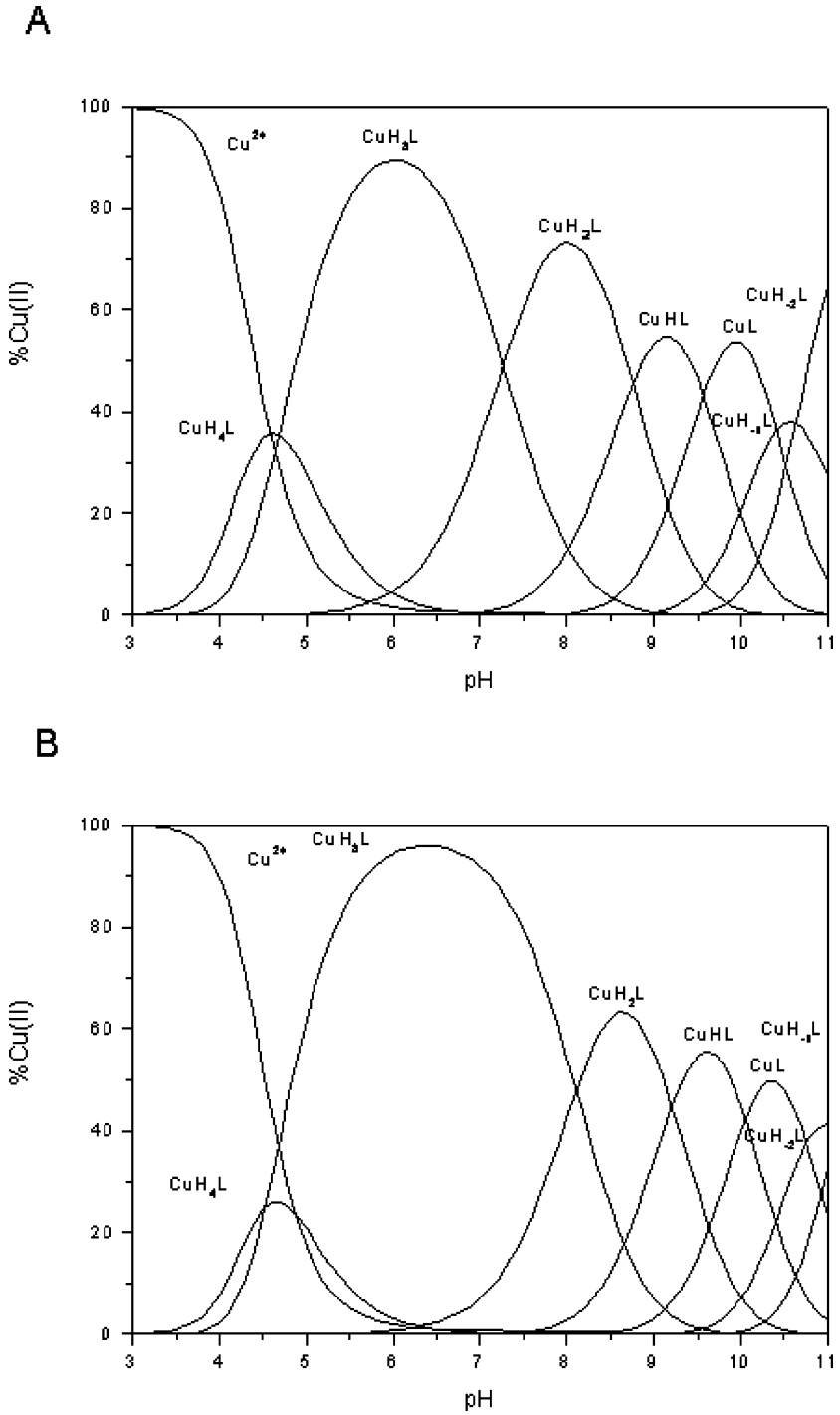

FIGURE 9: Species distribution profile for Cu^{2+} complexes of ChPrP(54−71) (A) and ChPrP(53−70) (B) at 298 K and $I = 0.1$ M KNO_3. $[Cu^{2+}] = 5 \times 10^{-4}$ M, metal/ligand ratio 1:1.

The same behavior was also found in human monomer, dimer and, tetramer octarepeats, where binding of more than one His was slowing down the kinetic dissociation rates (*31*). In particular, the human prion protein (HPrP) dimer octarepeat unit has a k_{off} (0.67 ms^{-1}) about 3 times slower than the monomer one (2.20 ms^{-1}) (*31*). All of these findings strongly suggest that inter-repeat binding of Cu^{II} is strongly favored in solutions having [Cu]/[peptide] $\leq$ 1, where the metal is bound to the His imidazole nitrogens of different units, as also observed with the human tetrarepeat unit (*40*).

The His H_ϵ R_{1p} values of the chicken and human prion dimers at the same ligand and metal concentrations were measured, and the corresponding k_{off} was then calculated by using eq 1, obtaining the values reported in Table 3 for ChPrP and those mentioned above for HPrP. Considering the relationship between the kinetic constant rates and the equilibrium constant

$$L + M \underset{k_{off}}{\overset{k_{on}}{\rightleftharpoons}} LM$$

$$K_{eq} = \frac{k_{on}}{k_{off}}$$

the ratio between the equilibrium constants of the human and chicken dimer repeats could be obtained, because the

Table 2

Potentiometric and Spectroscopic Data for Proton and Cu^{2+} Complexes of Ac-$(HNPGYP)_3$-NH_2, 3-Hex
Metal/Ligand Ratio = 1:1; $[Cu^{2+}] = 0.0005$ M

			UV−vis		CD		EPR	
species	log β	log K	λ (nm)	ϵ (M^{-1} cm^{-1})	λ (nm)	$\Delta\epsilon$ (M^{-1} cm^{-1})	$A_{\|\|}$ (G)	$g_{\|\|}$
Ac-$(HNPGYP)_3$-NH_2								
HL	10.62 (1)	log $K_{Tyr} = 10.62$						
H_2L	21.05 (1)	log $K_{Tyr} = 10.43$						
H_3L	30.53 (2)	log $K_{Tyr} = 9.48$						
H_4L	37.15 (1)	log $K_{im} = 6.62$						
H_5L	43.12 (3)	log $K_{im} = 5.97$						
H_6L	48.45 (2)	log $K_{im} = 5.33$						
CuH_4L	43.09 (2)		minor					
CuH_3L	38.01 (3)	4.68	659	33	629	−0.290	172	2.275
					279	−0.420		
CuH_2L	31.14 (4)	7.27	643	57	604	−0.022	172	2.273
					330	−0.159		
					279	−0.215		
					262	0.041		
CuHL	22.38 (4)	8.76	615	78	572	−0.140	172	2.272
					363	−0.220		
					279	0.516		
CuL	12.82 (5)	9.56	minor					
$CuH_{-1}L$	2.40 (5)	10.42	minor					
$CuH_{-2}L$	−8.23 (4)	10.63	570	69	630	0.015	190	2.241
					547	−0.089		
					327	0.684		

Potentiometric and Spectroscopic Data for Proton and Cu^{2+} Complexes of Ac-$(PHNPGY)_3$-NH_2, 3-Pex
Metal/Ligand Ratio = 1:1; $[Cu^{2+}] = 0.0005$ M

			UV−vis		CD		EPR	
species	log β	log K	λ (nm)	ϵ (M^{-1} cm^{-1})	λ (nm)	$\Delta\epsilon$ (M^{-1} cm^{-1})	$A_{\|\|}$ (G)	$g_{\|\|}$
Ac-$(PHNPGY)_3$-NH_2								
HL	10.92 (1)	log $K_{Tyr} = 10.92$						
H_2L	21.46 (1)	log $K_{Tyr} = 10.54$						
H_3L	31.26 (2)	log $K_{Tyr} = 9.80$						
H_4L	37.86 (2)	log $K_{im} = 6.60$						
H_5L	43.85 (2)	log $K_{im} = 5.99$						
H_6L	49.22 (1)	log $K_{im} = 5.37$						
CuH_4L	43.53 (3)		minor					
CuH_3L	39.01 (4)	4.52	641	64	601	0.056	178	2.271
					275	−0.700		
CuH_2L	30.90 (4)	8.11	636	87	602	−0.068	176	2.267
					337	−0.164		
					284	0.936		
CuHL	21.69 (4)	9.21	629	108	598	−0.125	176	2.268
					378	−0.214		
					282	1.227		
					255	2.529		
CuL	11.63 (5)	10.06	minor					
$CuH_{-1}L$	0.88 (5)	10.75	minor					
$CuH_{-2}L$	−10.22 (4)	11.10	552	108	631	0.073	178	2.262
					521	−0.239		
					323	0.457		

value of k_{on}, depending only on the diffusion process, can be considered the same for the two samples

$$\frac{K_{(\text{H Pr P\_dimer})}}{K_{(\text{Ch Pr P\_dimer})}} = \frac{k_{\text{off(Ch Pr P\_dimer)}}}{k_{\text{off(H Pr P\_dimer)}}} \cong 4$$

It can be therefore suggested that, as in the case of the monomer, the human prion dimer displays a slightly stronger affinity toward Cu^{II}. Such a conclusion is supported by the diverse impact of k_{off} on NMR line widths (Figure 12): the faster dissociation rate of ChPrP from the metal coordination sphere yields larger line broadening if compared with HPrP at the same Cu^{II}/ligand ratios. The fact that HPrP is not much stronger than ChPrP as a ligand toward Cu^{II} is further supported by the simultaneous line broadening experienced by both peptides in the presence of Cu^{II} (Figure 12E).

Potentiometric titrations and UV−vis, CD, and EPR spectroscopies were revealing for understanding the propensity of dimeric and trimeric units in accommodating more than one Cu^{II} ion. At 2:1 Cu^{II}/peptide ratios, both ChPrP(54−71) and ChPrP(53−70) were in fact forming several complexes with two Cu^{2+} ions bound to a single trimeric unit (Table 5S in the Supporting Information and Figure 10). Three imidazole nitrogen donors are involved in the coordination of two metal ions in the Cu_2H_3L complex, having all three Tyr oxygens protonated. The binding of two Cu^{II}

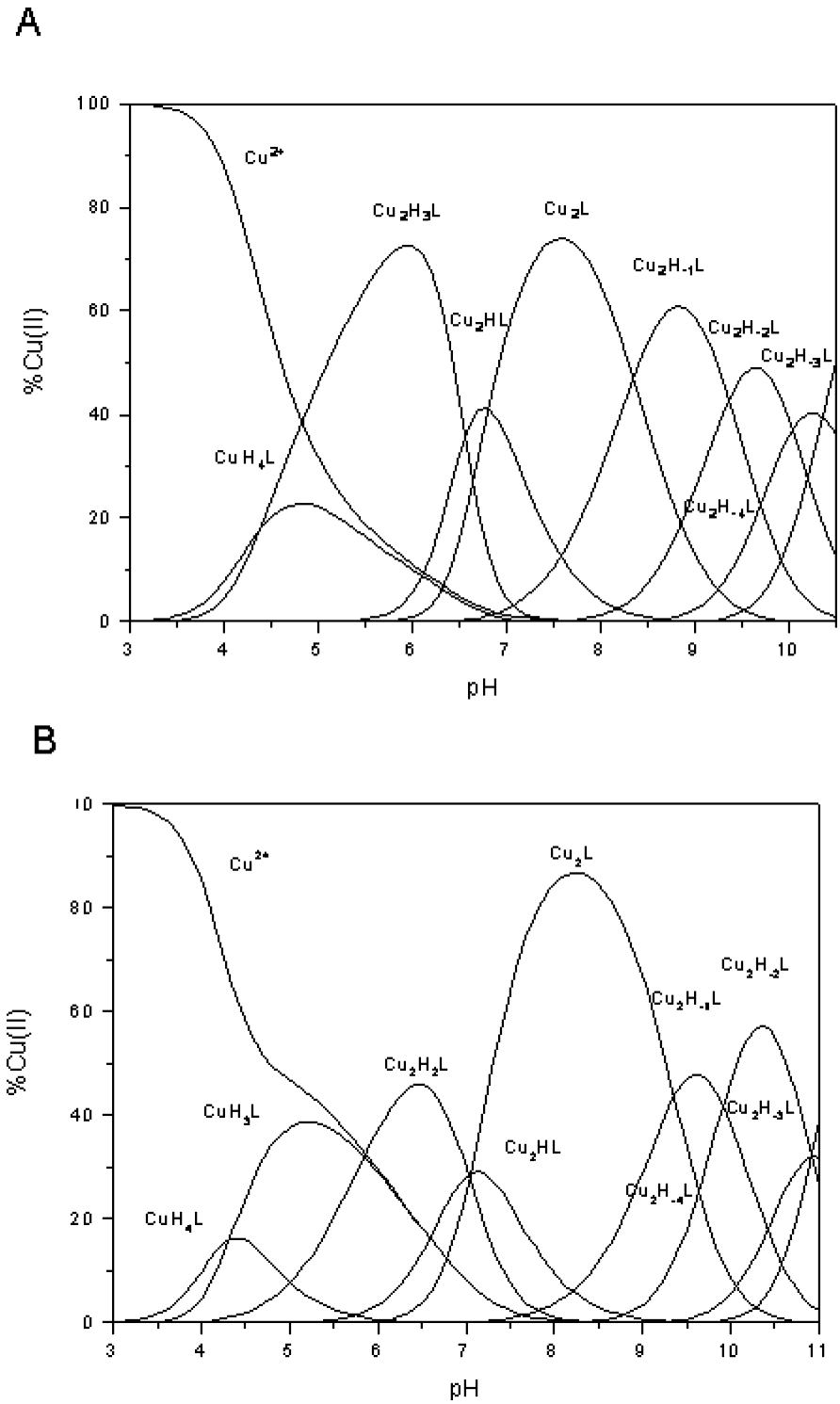

FIGURE 10: Species distribution profile for Cu^{2+} complexes of ChPrP(54−71) (A) and ChPrP(53−70) (B) at 298 K and $I = 0.1$ M KNO_3. $[Cu^{2+}] = 1 \times 10^{-3}$ M, metal/ligand ratio 2:1

ions to ChPrP(54−71) in Cu_2H_3L results in a very high value of (Log K^*_1 + log K^*_2) = 11.4. In the pH range of 7−8, the major complex is the Cu_2L species. This stoichiometry may be revealing for a coordination mode consisting of the three imidazole side chains, of two amide nitrogen donors, as well as of the deprotonation and binding (lower pK value) of one Tyr phenolate. It can be supposed that one Cu^{II} binds through two imidazole nitrogens and one amide nitrogen, whereas one imidazole nitrogen, one amide nitrogen, and the phenolate oxygen separately provide the binding donors for the second Cu^{II}. At 3:1 Cu^{II}/peptide ratios, at physiological pH, two predominant species are observed for the two peptides [$Cu_3H_{-2}L$ for ChPrP(54−71) and $Cu_3H_{-1}L$ for ChPrP(53−70)] with three Cu^{2+} ions bound to a single trimeric peptide (Figure 11), suggesting that each repeat binds one copper ion, in analogy with the binding mode found for the human octarepeat region (*9*, *14*, *15*).

Conclusions

Our results suggest that chicken hexarepeats exhibit a relatively large affinity toward copper. The structures of these complexes are different from those obtained for the human prion repeats, but metal binding is cooperative, just as

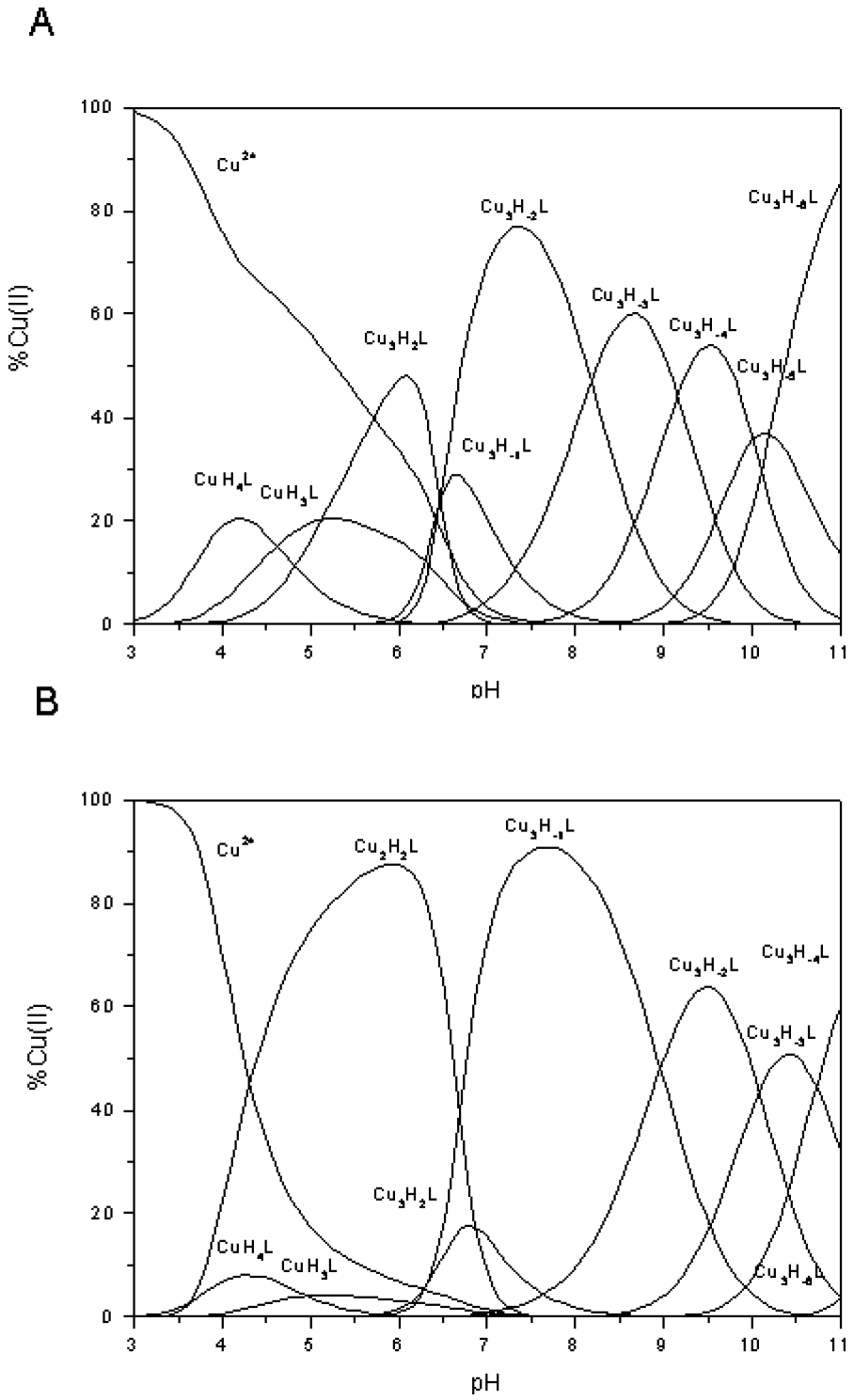

FIGURE 11: Species distribution profile for Cu^{2+} complexes of ChPrP(54−71) (A) and ChPrP(53−70) (B) at 298 K and $I = 0.1$ M KNO_3. $[Cu^{2+}] = 1.5 \times 10^{-3}$ M, metal/ligand ratio 3:1.

Table 3: Paramagnetic Relaxation Contributions R_{1p} and Exchange Rate Values (k_{off}) for Imidazole Protons of the Ac-HNPGYP-NH_2, ChPrP(54−59); Ac-$(HNPGYP)_2$-NH_2, ChPrP(54−65); and Ac-$(HNPGYP)_3$-NH_2, ChPrP(54−71) Cu^{II} Complexes, at $T = 298$ K

	R_{1p} (s^{-1})			k_{off} (s^{-1})		
Cu^{II} equiv	ChPrP(54−59)	ChPrP(54−65)	ChPrP(54−71)	ChPrP(54−59)	ChPrP(54−65)	ChPrP(54−71)
0.01	45	22	9.2	5000	2500	909
0.02	nd	55	20	nd	2500	1000
0.05	nd	142	34	nd	2500	668

observed for the human prion peptide sequence are revealing for the same mechanism for cooperativity of metal binding. The binding modes of ChPrP(54−59) and ChPrP(53−58) were found very similar to each other and involve one imidazole and one deprotonated His amide nitrogen at physiological pH, as supported by NMR and potentiometric titrations.

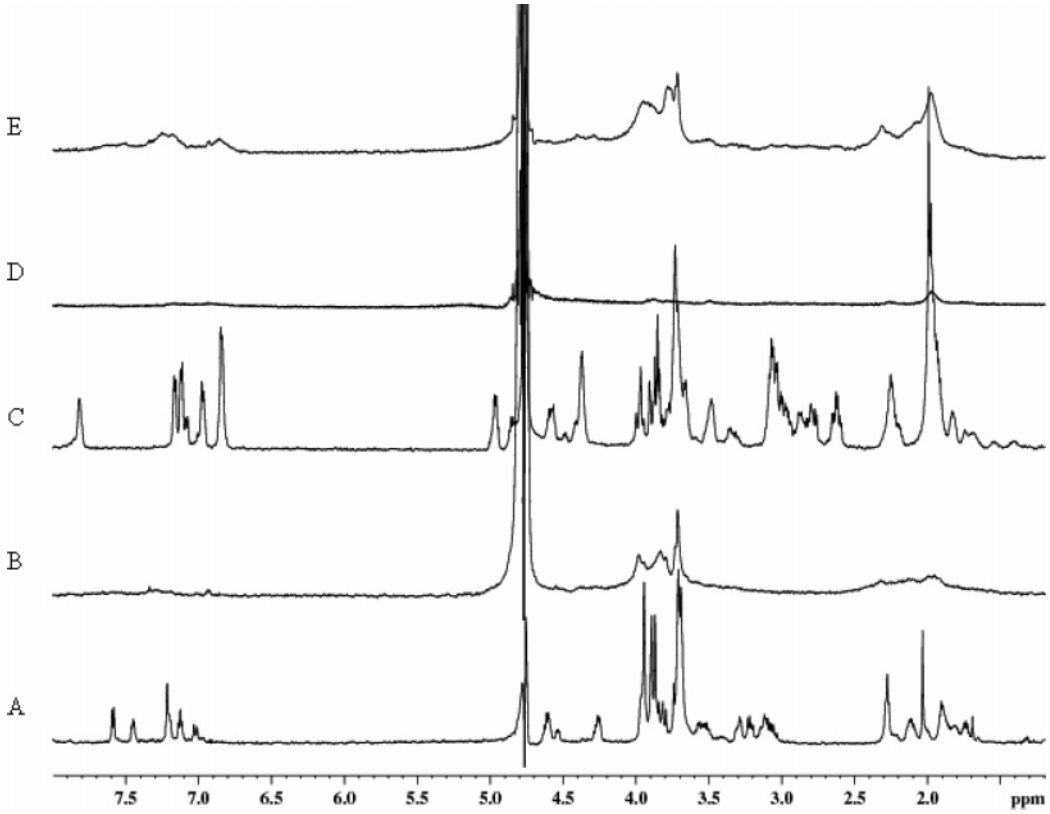

FIGURE 12: ^{1}H 600 MHz spectrum of in D_2O at pD 7.3 and $T = 298$ K: (A) 1 mM HPrP(61−76); (B) 1:1 HPrP(61−76)/Cu^{II}; (C) 1 mM ChPrP (54−65); (D) 1:1 ChPrP(54−65)/Cu^{II}; and (E) 1:1:1 HPrP(61−76)/ChPrP(54−65)/Cu^{II}.

In the case where two [ChPrP(54−65)] or three [ChPrP-(54−71)] repeats are considered at equimolar solutions, an inter-repeat copper coordination mode was observed. At physiological pH, copper binds cooperatively to two [ChPrP-(54−65)] or three [ChPrP(54−71)] imidazolic nitrogens.

The present findings demonstrate that, as for the human prion repeat (*40*), also the chicken prion repeat might bind copper in two different ways, depending on the number of repeats and the metal/ligand ratio, originating two types of Cu^{II} sites: (i) An intra-repeat coordination, where Cu^{II} is bound to His imidazole and deprotonated amide nitrogen, found for the monomeric peptide. (ii) An inter-repeat coordination, where only His imidazole nitrogens are bound to the metal ion, found in the dimeric and trimeric peptides at a Cu^{II}/ligand ratio ≤ 1.

The strong analogy between the human and chicken tandem repeat region in copper binding suggests a similar biological function for the two full-length proteins and strengthens the view that the relative amount of Cu^{II} determines whether the intra- or inter-repeat binding mode dominates (*40*).

SUPPORTING INFORMATION AVAILABLE

^{1}H and ^{13}C NMR assignments of the investigated peptides; the copper(II)−proton distances for the Cu^{II}−ChPrP(54−65) complex; paramagnetic relaxation contribution and distances for imidazole protons of the ChPrP(54−71) Cu^{II} complex; potentiometric and spectroscopic data for proton and Cu^{II} complexes of ChPrP(54−71) and ChPrP(53−70) at a metal/ligand ratio of 2:1; and distribution profiles of Cu^{II}-binding competition between ChPrP(54−59) and ChPrP-(53−58) and between ChPrP(54−71) and ChPrP(53−70). This material is available free of charge via the Internet at http://pubs.acs.org.

REFERENCES

1. Prusiner, S. B. (1982) Novel proteinaceous infectious particles cause scrapie, *Science 216*, 136−144.
2. Hegde, R. S., and Rane, N. S. (2003) Prion protein trafficking and the development of neurodegeneration, *Trends Neurosci. 26*, 337−339.
3. Borchelt, D. R., Scott, M., Taraboulos, A., Stahl, N., and Prusiner, S. B. (1990) Scrapie and cellular prion proteins differ in their kinetics of synthesis and topology in cultured cells, *J. Cell Biol. 110*, 743−752.
4. Borchelt, D. R., Taraboulos, A., and Prusiner, S. B. (1992) Evidence for synthesis of scrapie prion proteins in the endocytic pathway, *J. Biol. Chem. 267*, 16188−16199.
5. Harris, D. A., Falls, D. L., Johnson, F. A., and Fischbach, G. D. (1991) A prion-like protein from chicken brain copurifies with an acetylcholine receptor-inducing activity, *Proc. Natl. Acad. Sci. U.S.A. 88*, 7664−7668.
6. Wopfner, F., Weidenhöfer, G., Schneider, R., Von Brunn, A., Gilch, S., Schwarz, T. F., Werner, T., and Schätzl, H. M. (1999) Analysis of 27 mammalian and 9 avian PrPs reveals high conservation of flexible regions of the prion protein, *J. Mol. Biol. 289*, 1163−1178.
7. Brown, D. R., Qin, K., Herms, J. W., Madlung, A., Manson, J., Strome, R., Fraser, P. E., Kruck, T., von Bohlen, A., Schulz-Schaeffer, W., Glese, A., Westway, D., and Kretzschmar, H. (1997) The cellular prion protein binds copper *in vivo*, *Nature 390*, 684−687.
8. Millhauser, G. L. (2004) Copper binding in the prion protein, *Acc. Chem. Res. 37*, 79−85.
9. Brown, D. R., and Kozlowski, H. (2004) Biological inorganic and bioinorganic chemistry of neurodegeneration based on prion and Alzheimer diseases, *Dalton Trans.* 1907−1917.
10. Brown, D. R., Wong, B. S., Hafiz, F., Clive, C., Haswell, S. J., and Jones, I. M. (1999) Normal prion protein has an activity like that of superoxide dismutase, *Biochem. J. 344*, 1−5.

11. Burns, C. S., Aronoff-Spencer, E., Dunham, C. M., Lario, P., Avdievich, N. I., Antholine, W. E., Olmstead, M. M., Vrielink, A., Gerfen, G. J., Peisach, J., Scott, W. G., and Millhauser, G. L. (2002) Molecular features of the copper binding sites in the octarepeat domain of the prion protein, *Biochemistry 41*, 3991−4001.
12. Luczkowski, M., Kozlowski, H., Slawikowski, M., Rolka, K., Gaggelli, E., Valensin, D., and Valensin, G. (2002) Is the monomeric prion octapeptide repeat PHGGGWGQ a specific ligand for Cu^{2+} ions? *J. Chem. Soc., Dalton Trans.* 2269−2274.
13. Luczkowski, M., Kozlowski, H., Legowska, A., Rolka, K., and Remelli, M. (2003) The possible role of Gly residues in the prion octarepeat region in the coordination of Cu^{2+} ions, *Dalton Trans.* 619−624.
14. Garnett, A. P., and Viles, J. H. (2003) Copper binding to the octarepeats of the prion protein. Affinity, specificity, folding, and cooperativity: Insights from circular dichroism, *J. Biol. Chem. 278*, 6795−6802.
15. Valensin, D., Luczkowski, M., Mancini, F. M., Legowska, A., Gaggelli, E., Valensin, G., Rolka, K., and Kozlowski, H. (2004) The dimeric and tetrameric octarepeat fragments of prion protein behave differently to its monomeric unit, *Dalton Trans.* 1284−1293.
16. Hornshaw, M. P., McDermott, J. R., and Candy, J. M. (1995) Copper binding to the N-terminal tandem repeat regions of mammalian and avian prion protein, *Biochem. Biophys. Res. Commun. 207*, 621−629.
17. Stanczak, P., Luczkowski, M., Juszczyk, P., Grzonka, Z., and Kozlowski, H. (2004) Interactions of Cu^{2+} ions with chicken prion tandem repeats, *Dalton Trans.* 2102−2107.
18. Redecke, L., Meyer-Klaucke, W., Koker, M., Clos, J., Georgieva, D., Genov, N., Echner, H., Kalbacher, H., Perbandt, M., Bredehorst, R., Voelter, W., and Betzel, C. (2005) Comparative analysis of the human and chicken prion protein copper binding regions at pH 6.5, *J. Biol. Chem. 280*, 13987−13992.
19. Stañczak, P., Valensin, D., Juszczyk, P., Grzonka, Z., Valensin, G., Bernardi, F., Molteni, E., Gaggelli, E., and Kozlowski, H. (2005) Finetuning the structure of the Cu^{2+} complex with the prion protein chicken repeat by praline isomerization, *Chem. Commun. 26*, 3298−3300.
20. La Mendola, D., Bonomo, R. P., Impellizzeri, G., Maccarrone, G., Pappalardo, G., Pietropaolo, A., Rizzarelli, E., and Zito, V. (2005) Copper(II) complexes with chicken prion repeats: Influence of proline and tyrosine residues on the coordination features, *J. Biol. Inorg. Chem.*, PMID: 15926068.
21. Calzolai, L., Lysek, D. A., Perez, D. R., Guntert, P., and Wuthrich, K. (2005) Prion protein NMR structures of chickens, turtles, and frogs, *Proc. Natl. Acad. Sci. U.S.A. 102*, 651−655.
22. Zahn, R. (2003) The octapeptide repeats in mammalian prion protein constitute a pH-dependent folding and aggregation site, *J. Mol. Biol. 334*, 477−488.
23. Atherton, E., and Sheppard, R. C. (1989) *Solid-Phase Peptide Synthesis* (Rickwood, D., and Hames, B. D., Eds.) IRL Press, Oxford, U.K.
24. Fields, G. B., and Noble, R. L. (1990) Solid-phase peptide synthesis utilizing 9-fluorenylmethoxycarbonyl amino acids, *Int. J. Pept. Protein Res. 35*, 161−214.
25. Gran, G. (1950) Determination of the equivalent point in potentiometric titrations, *Acta Chem. Scand. 4*, 559−577.
26. Irving, H., Miles, M. G., and Pettit, L. D. (1967) A study of some problems in determining the stoicheiometric proton dissociation constants of complexes by potentiometric titrations using a glass electrode, *Anal. Chim. Acta 38*, 475−488.
27. Gans, P., Sabatini, A., and Vacca, A. (1985) SUPERQUAD: An improved general program for computation of formation constants from potentiometric data, *J. Chem. Soc., Dalton Trans*. 1195−1200.
28. Gans, P., Sabatini, A., and Vacca, A. (1996) Investigation of equilibria in solution. Determination of equilibrium constants with the HYPERQUAD suite of programs, *Talanta 43*, 1739−1753.
29. Güntert, P., Mumenthaler, C., and Wüthrick, K. (1997) Torsion angle dynamics for NMR structure calculation with the new program DYANA, *J. Mol. Biol. 273*, 283−298.
30. Pettit, L. D., Gregor, J. E., and Kozlowski, H., (1991) in *Perspectives on Bioinorganic Chemistry* (Hay, R. W., Dilworth, J. R., and Nolan, K. B., Eds.) Vol. 1, pp 1−41, JAI Press, London, U.K.
31. Gaggelli, E., Kozlowski, H., Valensin, D., and Valensin, G. (2005) NMR studies on Cu^{II}−peptide complexes: Exchange kinetics and determination of structures in solution, *Mol. BioSystems 1*, 79−84.
32. Pettit, D., Steel, I., Kowalik, T., Kozlowski H., and Bataille, M. (1985) Specific binding of the tyrosine residue in copper(II) complexes of Tyr-Pro-Gly-Tyr and Tyr-Gly-Pro-Tyr, *J. Chem. Soc., Dalton Trans. 6*, 1201−1205.
33. Kozlowski, H. (1983) *Proceedings of the 9th Conference on Coordination Chemistry*, Smolenice, Bratislava, p 201.
34. Bataille, M., Formicka-Kozlowska, G., Kozlowski, H., Pettit, L. D., and Steel, I. (1984) The L-proline residue as a break-point in the co-ordination of metal−peptide systems, *J. Chem. Soc. Chem. Commun. 4*, 231−232.
35. Kozlowski, H., Bal, W., Dyba, M., and Kowalik-Jankowska, T. (1999) Specific structure−stability relations in metallopeptides, *Coord. Chem. Rev. 184*, 319−346.
36. Gaggelli, E., D'Amelio, N., Valensin, D., and Valensin, G. (2003) ^{1}H NMR studies of copper binding by histidine-containing peptides, *Magn. Reson. Chem. 41*, 877−883.
37. Gaggelli, E., Bernardi, F., Molteni, E., Pogni R., Valensin, D., Valensin, G., Remelli, M., Luczkowski, M., and Kozlowski, H. (2005) Interaction of the human prion PrP(106−126) sequence with copper(II), manganese(II), and zinc(II): NMR and EPR studies, *J. Am. Chem. Soc. 127*, 996−1006.
38. Bertini, C., Luchinat, G., and Parigi (2001) Solution NMR of paramagnetic molecules application to metallobiomolecules and models, in *Current Methods in Inorganic Chemistry*, Vol. 2, Elsevier, The Netherlands.
39. Solomon, I. (1955) Relaxation processes in a system of two spins, *Phys. Rev. 99*, 559−565.
40. Morante, S., González-Iglesias, R., Potrich, C., Meneghini, C., Meyer-Klaucke, W., Menestrina, G., and Gasset, M. (2004) Inter- and intra-octarepeat Cu^{II} site geometries in the prion protein: Implications in Cu^{II} binding cooperativity and Cu^{II}-mediated assemblies, *J. Biol. Chem. 279*, 11753−11759.

BI051177E